Circular Polarization Microstrip Antenna on a Conical Surface

Reuven Shavit, *Senior Member, IEEE*

***Abstract*—A theoretical model to analyze the performance of a circular polarization microstrip antenna printed on a conical surface is presented. The radiation pattern of the antenna is simulated by the radiation from its four radiating edges (two axial and two circumferential). The electromagnetic field is expanded in terms of spherical wave modes and it is shown that the circular polarization is obtained by exciting in the antenna two spherical TE_r orthogonal modes with 90° phase difference. The impedance analysis is based on the cavity model. Experimental data fits well the theoretical predictions of the model.**

***Index Terms*—Microstrip antennas.**

I. Introduction

ANTENNA elements based on microstrip technology are low profile, conformable, low weight, and low cost. As such, they are commonly used in many applications. Lately, extensive effort was devoted to compute the radiation characteristics of microstrip elements on flat and cylindrical surfaces [1]–[4] for both linear and circular polarization, but only minor attention has been given to the analysis of microstrip elements on a conical surface, which is of a significant importance in satellite and space communication. Newham and Morris [5] gave a review on the practical aspects of designing a conical conformable microstrip-tracking antenna. The antenna parameters on the conical surface were approximated by considering an equivalent flat rectangular patch. Descardeci and Giarola [6] analyzed the performance of a linear polarization patch antenna on a conical surface by using dyadic Green's function and the radiated field was expanded by *vector wave functions*. The analysis is general, but mathematically involved, and does not contain the approximations usually made for thin patch antennas, which significantly simplify the computations.

In this paper, we have expanded the radiated field in TM_r and TE_r *spherical modes*. This approach combined with application of Lorentz reciprocity theorem simplified significantly the radiation pattern mathematical expressions. The computation of the radiated field by axial and circumferential magnetic currents was performed in a similar fashion to that described by Bailin and Silver [7]. We used the cavity model with the approximations made for a low-height cavity to compute the internal field under the patch and the input impedance. In the cavity model we considered the fringing field at the patch edges. The circular polarization of the microstrip element was obtained by exciting in the cavity two TE_r orthogonal modes with 90° phase difference among them. The radiated field from the antenna was obtained by superposing the radiation from four equivalent magnetic currents along the edges of the patch (two axial and two circumferential). We assumed that their distribution is determined by the two dominant modes excited in the cavity. Section II describes the theoretical approach to evaluate the resonant frequencies, the radiation field, and the input impedance. Section III compares theoretical and experimental results of the input impedance and illustrates the radiated field based on the model.

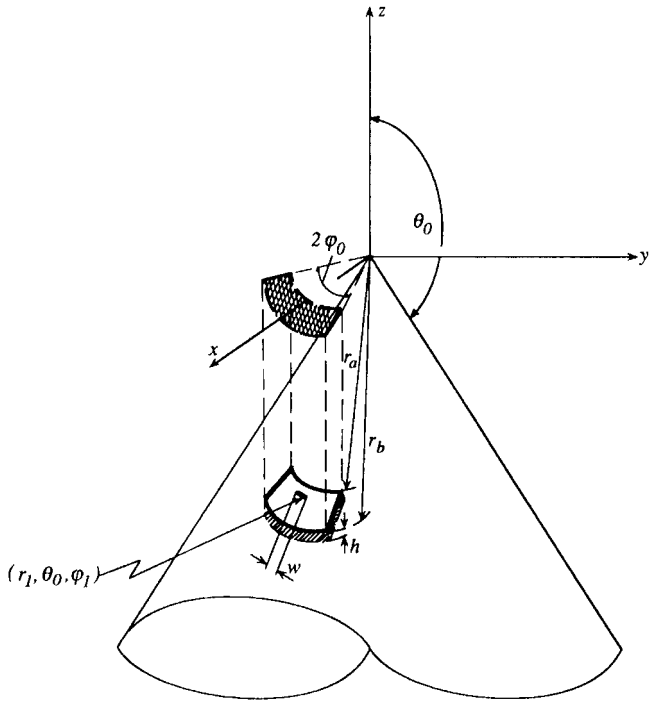

Fig. 1. The basic geometry of a patch antenna on a conical surface.

II. Theory

The basic geometry of a patch antenna on a conical surface is shown in Fig. 1. The angle between the cone axis and its surface is θ_0, the angular width of the patch is $2\phi_0$, and its length is $r_b - r_a$. The patch is printed on a dielectric substrate backed by a ground surface, which is wrapped around the cone. The substrate thickness is h and its dielectric constant is ε_r. The patch is fed by a coaxial cable at $r = r_1$ and $\phi = \phi_1$ modeled by a metal strip with effective width w.

Manuscript received June 19, 1995; revised July 26, 1996.

The author is with the Department of Electrical and Computer Engineering, Ben-Gurion University of the Negev, Beer Sheva, 84105 Israel.

Publisher Item Identifier S 0018-926X(97)04888-6.

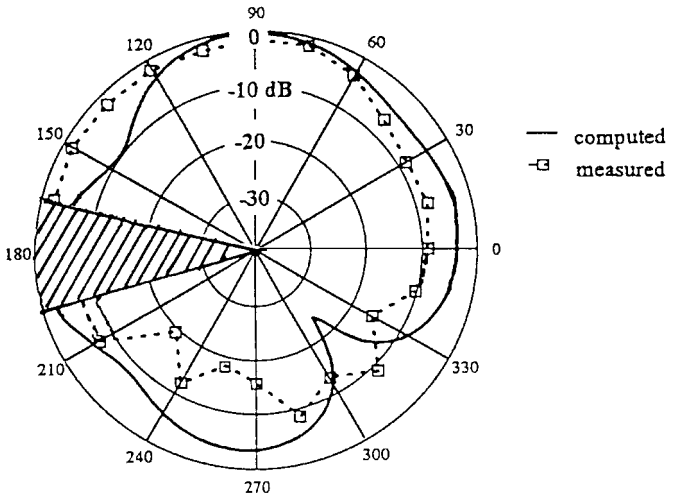

Fig. 2. The far-field normalized E_θ in the X–Z plane (computed and measured data).

A. Resonant Frequencies

The region between the patch and the conical surface is considered as a cavity bounded by electric walls on the top and bottom and by magnetic walls on the sides, as such it has resonant frequencies. The cavity radial length is extended by $2\Delta r$ and its transverse width by $2\Delta l$ to account for the fringing field at the edges. The approximation of Δr and Δl can be found in [8]. For a low-height cavity, the field inside can be expanded only in TE$_r$ modes. Accordingly, using spherical coordinates, the general solution of the electric vector potential F_r is given by [9]

$$\begin{aligned} F_r = &[A_n \hat{J}_n(kr) + B_n \hat{N}_n(kr)] \\ &\times \left[C_n P_n^m(\cos\theta) + D_n Q_n^m(\cos\theta)\right] \\ &\times [E_m \sin m\phi + F_m \cos m\phi] \end{aligned} \tag{1}$$

in which $\hat{J}_n(kr)$, $\hat{N}_n(kr)$ are Bessel functions used by Schelkunoff [9] and $P_n^m(\cos\theta)$, $Q_n^m(\cos\theta)$ are Legendre functions of first and second order, respectively. If we impose the boundary conditions of the electric walls on top and bottom walls, we obtain the characteristic equation

$$\begin{aligned} &P_n'^m(\cos\theta_0)Q_n'^m(\cos(\theta_0+\Delta\theta)) \\ &\quad - P_n'^m(\cos(\theta_0+\Delta\theta))Q_n'^m(\cos\theta_0) = 0 \end{aligned} \tag{2}$$

in which the prime denotes derivative. In a similar fashion, if we impose the boundary conditions on the magnetic walls of the cavity, we obtain two characteristics equations

$$\hat{J}_n'(k_l r_a)\hat{N}_n'(k_l r_b) - \hat{J}_n'(k_l r_b)\hat{N}_n'(k_l r_a) = 0 \tag{3}$$

and

$$\sin(2m\phi_0) = 0; \quad m = q\pi/2\phi_0; \quad q = 0, 1, 2, \cdots. \tag{4}$$

In addition, we obtain the general expression of the nml spherical mode in the cavity

$$\begin{aligned} F_r = C_{nml}&[\hat{N}_n'(k_l r_a)\hat{J}_n(k_l r) - \hat{J}_n'(k_l r_a)\hat{N}_n(k_l r)] \\ &\times [Q_n^m(\cos\theta_0)P_n^m(\cos\theta) - P_n^m(\cos\theta_0)Q_n^m(\cos\theta)] \\ &\times \sin m(\phi - \phi_0). \end{aligned} \tag{5}$$

Given F_r, we can compute the θ component of the electric field in the cavity [9]

$$E_\theta = -\frac{1}{r\sin\theta}\frac{\partial F_r}{\partial \phi}. \tag{6}$$

So far, the derivation is general and no simplifications have been done for our specific case in which $h \ll \lambda$. In this case, the excited field in the cavity is independent of θ ($\frac{\partial}{\partial\theta} = 0$). This fact leads to the observation that only modes with index $n = 0$ exist in the cavity. One can observe that in this case, (2) is satisfied for all m's. If we recall that [9] $\hat{J}_0(k_l r) = \sin k_l r$ and $\hat{N}_0(k_l r) = -\cos k_l r$, (3) can be further simplified with the result that $k_l = l\pi/(r_b - r_a)$ with $l = 0, 1, 2, \cdots$. This leads to a simplified expression of the E_θ component of the lq mode as derived from (6)

$$E_\theta = -\frac{q\pi}{2\phi_0 r\sin\theta}C_{lq}\cos\left(\frac{l\pi(r-r_a)}{r_b - r_a}\right)\cos\left(\frac{q\pi(\phi-\phi_0)}{2\phi_0}\right). \tag{7}$$

In addition, the assumption that $\frac{\partial}{\partial\theta} = 0$ also simplifies the free-source wave equation in the cavity

$$\nabla \times \nabla \times \underline{E} - k^2 \underline{E} = 0 \tag{8}$$

such that its θ component in spherical coordinates is

$$\frac{1}{r}\frac{\partial^2}{\partial r^2}(rE_\theta) + \frac{1}{r^2\sin^2\theta}\frac{\partial^2 E_\theta}{\partial\phi^2} + k^2 E_\theta = 0. \tag{9}$$

If we assume that the patch on the conical surface is close to a rectangular shape such that its transversal width can be approximated by

$$r\sin\theta_0 2\phi_0 \cong a = \frac{r_a + r_b}{2}\sin\theta_0 2\phi_0 \tag{10}$$

(9) can be further simplified and we obtain the eigenvalues satisfying the boundary conditions of our cavity

$$k^2 = k_{lq}^2 = \left(\frac{l\pi}{b_e}\right)^2 + \left(\frac{q\pi}{a_e}\right)^2 \tag{11}$$

in which b_e is the effective length of the patch and equals to $b_e = r_b - r_a + 2\Delta r$. Similarly, a_e is the effective width and equals to $a_e = a + 2\Delta l$. Accordingly, the expression for the resonant frequencies is

$$f_{lq} = \frac{c}{2\sqrt{\varepsilon_r}}\left[\left(\frac{l}{b_e}\right)^2 + \left(\frac{q}{a_e}\right)^2\right] \tag{12}$$

where c is the velocity of light in free space. Equation (12) shows that if the dimensions of the patch, i.e., a_e and b_e, are fixed, the resonant frequencies of the TE$_r$ modes are not affected by the curvature. This conclusion is valid for thin substrates.

B. Radiation Field

The radiated field from the patch can be obtained by superposing the radiation from four equivalent slots along its edges (two axial and two circumferential) and located at a height h above the ground plane. The lengths of the circumferential slots are $r_a \sin\theta_0 2\phi_0$ and $r_b \sin\theta_0 2\phi_0$ and their width is Δr. The length of the axial slots is $r_b - r_a$ and their width is Δl.

The radiation from the slots is equivalent (by Schelkunoff principle) to that of equivalent magnetic currents $\underline{J}_m = -\underline{1}_n \times \underline{E}_s$ in which $\underline{E}_s$ is the electric field at the patch edges for the two dominant and orthogonal modes ($l = 0$, $q = 1$ and $l = 1$, $q = 0$) generated under the patch and $\underline{1}_n = \underline{1}_\theta$. $\underline{E}_s$ can be approximated by the electric field on the cavity walls of the patch, as given by (7). $\underline{E}_s$ is r directed for the circumferential slots and ϕ directed for the axial slots. Accordingly, the magnetic currents are azimuthal for the circumferential slots and radial for the axial slots.

The radiated field from a magnetic current on the conical surface can be expanded in terms of TM_r and TE_r spherical modes [7]. Based on symmetry considerations, the radiation field by a circumferential slot can be expanded only in TM_r modes, while that for an axial magnetic current only in TE_r modes.

Thus, the magnetic vector potential A_r generated by an infinitesimal ϕ directed magnetic current located at (r', ϕ') on the conical surface can be expressed as (13), shown at the bottom of the page. Similarly, the electric vector potential F_r generated by an infinitesimal r directed magnetic current is (14), shown at the bottom of the page. In the expansion, we have not included the Legendre function $Q^m_{u_i}(\cos\theta)$ and the Bessel function $\hat{N}_{u_i}(k_0 r)$, since these functions diverge at $\theta = 0^\circ$ and $r = 0$, respectively. For $r > r'$, $\hat{J}_{u_i}(k_0 r)$ has been replaced by $\hat{H}^{(2)}_{u_i}(k_0 r)$ to satisfy the radiation condition at infinity. If we impose the boundary conditions of the tangential electric field on the conductive conical surface, we obtain for the TM_r modes the characteristic equation

$$P^m_{u_i}(\cos\theta_0) = 0 \tag{15}$$

while for the TE_r modes

$$P'^m_{v_i}(\cos\theta_0) = 0 \tag{16}$$

in which i, m are integers ($i, m = 0, 1, 2\cdots$), while u_i, v_i are not necessarily integers. The prime indicates derivative of the Legendre function. The relationship between the set of coefficients $A_{u_i,m}$, $B_{u_i,m}$ to $A'_{u_i,m}$, $B'_{u_i,m}$ and $C_{v_i,m}$, $D_{v_i,m}$ to $C'_{v_i,m}$, $D'_{v_i,m}$ is obtained by imposing continuity of the field at the interface $r = r'$. To determine the coefficients $A_{u_i,m}$, $B_{u_i,m}$, $C_{v_i,m}$, $D_{v_i,m}$, we apply the Lorentz reciprocity theorem in the form

$$\int_s (\underline{E}_1 \times \underline{H}_2) \cdot \underline{n}\, ds = \int_s (\underline{E}_2 \times \underline{H}_1) \cdot \underline{n}\, ds \tag{17}$$

in which $(\underline{E}_1, \underline{H}_1)$ is the actual field, while $(\underline{E}_2, \underline{H}_2)$ is any one of the spherical modes. The surface s consists from a spherical surface with radius $r\,(r \to \infty)$ bounded by the cone and the conical surface. If we proceed in this fashion and follow the derivation in [7], we obtain (after some algebraic manipulations) the expressions for the far-zone electric field of the circumferential slot at $r = r_a$

$$E_\theta = jE_a k_0 \Delta s_a \frac{e^{-jk_0 r}}{r} \sum_{i,m} j_{u_i}(k_0 r_a) \times \frac{\sin m\phi_0}{m\phi_0} \frac{(2u_i + 1) j^{u_i}}{\pi(1 + \delta_{0m}) u_i (u_i + 1) \sin\theta_0 \left.\frac{dP^m_{u_i}}{du_i}\right|_{\theta=\theta_0}} \times \frac{dP^m_{u_i}}{d\theta} \cos m\phi \tag{18}$$

and

$$E_\phi = -jE_a k_0 \Delta s_a \frac{e^{-jk_0 r}}{r} \sum_{i,m} j_{u_i}(k_0 r_a) \times \frac{\sin m\phi_0}{m\phi_0} \frac{(2u_i + 1) j^{u_i} m}{\pi(1 + \delta_{0m} u_i (u_i + 1) \sin\theta_0 \left.\frac{dP^m_{u_i}}{du_i}\right|_{\theta=\theta_0}} \times \frac{P^m_{u_i}(\cos\theta)}{d\theta} \sin m\phi \tag{19}$$

in which δ_{0m} is equal to one for $m = 0$ and equal to zero otherwise, $j_{u_i}(k_0 r)$ is a spherical Bessel function related to $\hat{J}_{u_i}(k_0 r)$ through $j_{u_i}(k_0 r) = \hat{J}_{u_i}(k_0 r)/k_0 r$ [9]. Δs_a is the area of the slot and equals to $r_a \sin\theta_0 2\phi_0 \Delta r$. E_a is the electric field on the cavity wall of the patch at $r = r_a$.

For the circumferential slot located at $r = r_b$, the index a is replaced with b. In a similar fashion, we obtain the radiated field for the axial slots

$$E_\theta = E_{\phi_0} \Delta\phi_0 \frac{e^{-jk_0 r}}{r} \sum_{i,m} \int_{r_a}^{r_b} j_{v_i}(k_0 r')\, dr' \times \frac{(2v_i + 1) j^{v_i} m}{\pi(1 + \delta_{0m}) \left.\frac{d^2 P^m_{v_i}}{d\theta\, dv_i}\right|_{\theta=\theta_0}} \frac{P^m_{v_i}(\cos\theta)}{\sin\theta} \sin m(\phi \pm \phi_0) \tag{20}$$

$$A_r = \begin{cases} \sum_{i,m} \hat{J}_{u_i}(k_0 r) P^m_{u_i}(\cos\theta)\left[A_{u_i,m} \cos m\phi + B_{u_i m} \sin m\phi\right]; & r < r' \\ \sum_{i,m} \hat{H}^{(2)}_{u_i}(k_0 r) P^m_{u_i}(\cos\theta)[A'_{u_i,m} \cos m\phi + B'_{u_i m} \sin m\phi]; & r > r' \end{cases} \tag{13}$$

$$F_r = \begin{cases} \sum_{i,m} \hat{J}_{v_i}(k_0 r) P^m_{v_i}(\cos\theta)\left[C_{v_i,m} \cos m\phi + D_{v_i m} \sin m\phi\right]; & r < r' \\ \sum_{i,m} \hat{H}^{(2)}_{v_i}(k_0 r) P^m_{v_i}(\cos\theta)\left[C'_{v_i,m} \cos m\phi + D'_{v_i m} \sin m\phi\right]; & r > r' \end{cases} \tag{14}$$

and

$$E_\phi = E_{\phi_0}\Delta\phi_0\frac{e^{-jk_0r}}{r}\sum_{i,m}\int_{r_a}^{r_b} j_{v_i}(k_0r')\,dr' \times \frac{(2v_i+1)j^{v_i}}{\pi(1+\delta_{0m})\frac{d^2P_{v_i}^m}{d\theta dv_i}\Big|_{\theta=\theta_0}}\frac{dP_{v_i}^m}{d\theta}\cos m(\phi\pm\phi_0). \quad (21)$$

For the purpose of the computation of the total radiation pattern of the patch, we consider the radiation from an array with four radiating elements, which are the equivalent slots. The center locations of the circumferential slots are at $(r_a\sin\theta_0,\ 0,\ r_a\cos\theta_0)$, and $(r_b\sin\theta_0,\ 0,\ r_b\cos\theta_0)$, while that of the axial slots are at $[(r_a+r_b)/2*\sin\theta_0*\cos\phi_0,\ \pm(r_a+r_b)/2*\sin\theta_0*\sin\phi_0,\ (r_a+r_b)/2*\cos\theta_0)]$. A quality factor for the circular polarization is the axial ratio [10]. Given the θ and ϕ components of the total field one can compute the axial ratio, AR of the radiated field (22), shown at the bottom of the page, where $\alpha=\tan^{-1}E_\theta/E_\phi$.

C. Input Impedance

Consider that the patch is fed by a coaxial cable at $r=r_1$ and $\phi=\phi_1$. In this case it can be modeled by a θ directed current strip of width w and angular extent $\Delta\phi$

$$J_\theta = J(\phi-\phi_1)\delta(r-r_1) \quad (23)$$

where

$$J(\phi-\phi_1)=\frac{I_0}{w}\begin{cases}1, & |\phi-\phi_1|\le\Delta\phi\\ 0, & \text{elsewhere}\end{cases} \quad (24)$$

I_0 is the input current to the patch and $w=r_1\sin\theta_0 2\Delta\phi$.

The electric field, E_θ under the patch can be expanded in terms of spherical TE$_r$ modes as given by (7), such that

$$E_\theta = -\frac{1}{r\sin\theta}\sum_{l,q}C_{l,q}\cos\frac{l\pi}{r_b-r_a}(r-r_a) \times\cos\frac{q\pi}{2\phi_0}(\phi-\phi_0). \quad (25)$$

Evaluation of the coefficients $C_{l,q}$ is possible if we substitute (25) into the wave equation in spherical coordinates ($\frac{\partial}{\partial\theta}=0$)

$$\frac{1}{r}\frac{\partial^2}{\partial r^2}(rE_\theta)+\frac{1}{r^2\sin^2\theta}\frac{\partial^2E_\theta}{\partial\phi^2}+k^2E_\theta = j\omega\mu J_\theta \quad (26)$$

multiply both sides by $\cos\frac{q'\pi}{2\phi_0}(\phi-\phi_0)\cos\frac{l'\pi}{r_b-r_a}(r-r_a)$ and integrate over the cavity volume under the patch. The result is

$$C_{l,q} = -j\omega\mu\frac{I_0}{2\phi_0 b_e}\frac{\cos\frac{l\pi}{b_e}(r_1-r_a)\cos\frac{q\pi}{2\phi_0}(\phi_0-\phi_1)\operatorname{sinc}\frac{q\pi\Delta\phi}{2\phi_0}}{\sigma_q\sigma_l\left[k_{\text{eff}}^2-\left(\frac{l\pi}{b_e}\right)^2-\left(\frac{q\pi}{a_e}\right)^2\right]} \quad (27)$$

in which σ_q equals one for $q=0$ and 1/2, otherwise. In (27), k has been replaced by k_{eff}

$$k_{\text{eff}} = k_0\sqrt{\varepsilon_r(1-j\tan\delta_{\text{eff}})},\qquad k_0=\omega\sqrt{\mu_0\varepsilon_0} \quad (28)$$

in which $\tan\delta_{\text{eff}}$ accounts for the radiation, dielectric, copper, and surface wave losses of the cavity and is computed from the expression

$$\tan\delta_{\text{eff}} = \tan\delta\left(1+\frac{P_r}{P_d}+\frac{P_c}{P_d}+\frac{P_{\text{sw}}}{P_d}\right) \quad (29)$$

where $\tan\delta$ is the loss tangent of the dielectric material in the cavity, P_r is the radiated power, P_d is the power dissipated in the dielectric material, P_c is the power dissipated on top and bottom walls, and P_{sw} is the power dissipated on surface waves. The total Q quality factor is equal to $1/\tan\delta_{\text{eff}}$. Usually, for thin patches, the copper and surface wave losses are negligible compared to the radiation losses. The total radiated power is the superposition of the radiated power from the four equivalent slots around the patch. Each one of them can be computed by integrating the Poynting vector of the radiated far field

$$P_r = \frac{1}{2\eta}\int_0^{\theta_0}\int_0^{2\pi}(|E_\theta|^2+|E_\phi|^2)r^2\sin\theta\,d\theta\,d\phi \quad (30)$$

in which $\eta=120\pi$ and E_θ, E_ϕ are the far-zone radiated electric fields given by (18)–(21) for the axial and circumferential slots. The power dissipated in the dielectric can be computed by integrating the power in the patch cavity volume

$$P_d = \frac{1}{2}\omega\varepsilon_0\varepsilon_r\tan\delta h\int_{r_a}^{r_b}\int_{-\phi_0}^{\phi_0}|E_\theta|^2 r\sin\theta\,d\phi\,dr. \quad (31)$$

Here, E_θ is the electric field in the cavity and is given by (25). The input impedance is obtained by evaluating the integral [1]

$$Z_{\text{in}} = -\frac{h}{I_0^2}\int_{\phi_1-\Delta\phi}^{\phi_1+\Delta\phi}E_\theta|_{r=r_1}\cdot J_\theta\cdot r_1\sin\theta_0\,d\phi \quad (32)$$

in which E_θ is given by (25) and J_θ is given by (23).

The result is

$$Z_{\text{in}} = -j\omega\mu\frac{h}{a_eb_e} \times\sum_{l,q}\frac{\cos^2\frac{l\pi}{b_e}(r_1-r_a)\cos^2\frac{q\pi}{2\phi_0}(\phi_0-\phi_1)\operatorname{sinc}^2\frac{q\pi\Delta\phi}{2\phi_0}}{\sigma_q\sigma_l\left[k_{\text{eff}}^2-\left(\frac{l\pi}{b_e}\right)^2-\left(\frac{q\pi}{a_e}\right)^2\right]}. \quad (33)$$

$$\text{AR} = \left[\frac{|E_\theta|^2+|E_\phi|^2+(|E_\theta|^4+|E_\theta|^4+2|E_\theta|^2|E_\theta|^2\cos2\alpha)^{1/2}}{|E_\theta|^2+|E_\phi|^2-(|E_\theta|^4+|E_\theta|^4+2|E_\theta|^2|E_\theta|^2\cos2\alpha)^{1/2}}\right]^{1/2} \quad (22)$$

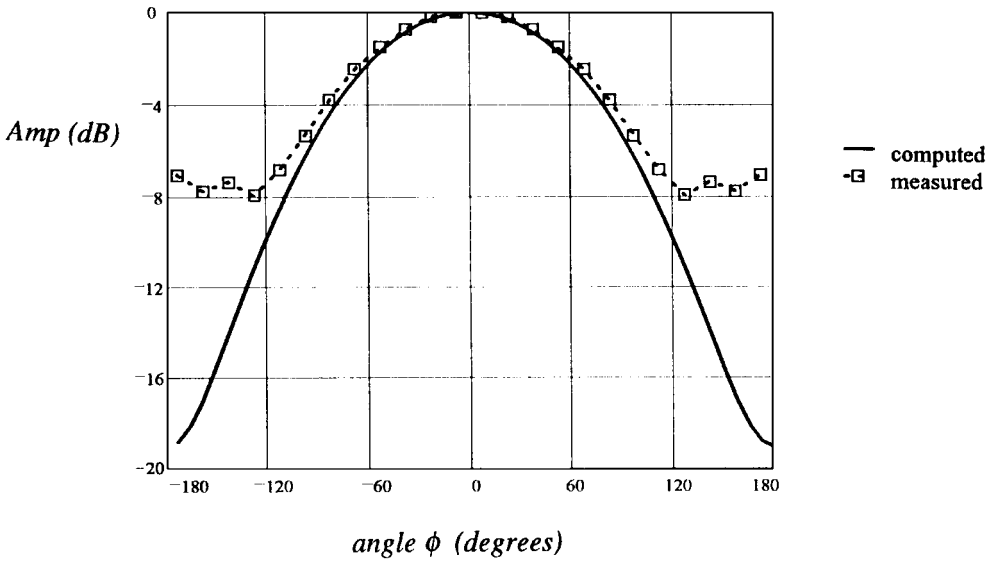

Fig. 3. The normalized far-field E_θ dependence on ϕ for $\theta = 75^\circ$ (peak of radiation pattern).

III. Numerical Results

In the computation of the radiation pattern of the patch, we have encountered several mathematical difficulties due to the nonintegral value of u_i, v_i in the characteristic equations (15) and (16). The first was in the computation of these values. An approximation for θ_0 close to π (our case) can be found in [11] (34), shown at the bottom of the page, and

$$v_i = i + \frac{\Gamma(2m+i+3)}{\Gamma(m+1)\Gamma(m+2)\Gamma(i+1)} \cdot \left(\frac{\pi-\theta_0}{3}\right)^{2(m+1)} \qquad m = 0, 1\cdots; \quad i = 1, 2\cdots \tag{35}$$

in which $\Gamma(x)$ is the Gamma function [12]. Based on these initial values the exact values of u_i, v_i have been found by using a standard root-finding algorithm. The second difficulty was encountered in the computation of the Legendre function and its derivatives. Use of the standard summation formulas found in [12] gave nonconvergent value and we had to use Stirling formula [12] to obtain a better convergence. The result is

$$P_u^m(z) = \frac{1}{\Gamma(-u)\Gamma(1+u)}\left(\frac{1+z}{1-z}\right)^{\frac{m}{2}} \times \left[\sum_{n=0}^{N} \frac{\Gamma(n-u)\Gamma(1+u+n)(1-z)^n}{\Gamma(1-m+n)2^n n!} + \sum_{n=N+1}^{\infty} \frac{(1-z)^n}{n2^n}\right]. \tag{36}$$

The derivative of $P_u^m(z)$ with respect to z has been found by using recurrence formula as shown in [12], while the derivative with respect to u has been found by taking the derivative of (36) and use of the asymptotic expressions for large index values to speed up convergence.

As a test case, we examined a microstrip antenna printed on a conical surface with $\theta_0 = 165.2^\circ$. The patch was printed on a substrate with $h = 0.075''$, $\varepsilon_r = 10.2$, $\tan\delta = 0.0017$, and with dimensions $r_a = 7.68$ cm, $r_b = 10.49$ cm, and $\phi_0 = 34^\circ$. The antenna was fed by a coaxial line through the ground of the conical surface. The probe was simulated by a strip with a width of 0.15 cm located at $r_1 = 9.37$ cm, $\phi_1 = 6.7^\circ$ and the operating frequency is 1.59 GHz. Due to practical limitations the patch was assembled on a truncated aluminum conical surface with a length of 30 cm.

Fig. 2 shows the normalized electric far-field component E_θ (measured and computed) radiated by the patch in the *X–Z plane* (elevation). The peaks of the two radiation patterns coincide and their shapes follow closely. As expected, the peak of the radiation pattern of the patch on the conical surface occurs close to 75° from its axis. Moreover, one can observe that in the lower hemisphere there is a significant amount of radiation, which cannot be predicted by a flat surface patch model. Fig. 3 shows the dependence of the normalized far-field component E_θ (measured and computed) on ϕ for $\theta = 75^\circ$ (peak of the radiation pattern). The computed pattern follows closely the measured up to $\pm 120^\circ$. Beyond this angle there is a discrepancy between the measured and computed data due measurement error in the alignment of the measurement setup. Fig. 4 shows the dependence of the axial ratio (measured and computed) in the X–Z plane for $\phi = 0^\circ$. As expected, the best axial ratio occurs close to 75° and deteriorates on both sides of the peak radiation. One can observe a nice agreement between the measured and computed data in the range of 50°

$$u_i = \begin{cases} i + \frac{1}{2\ln\left(\frac{2}{\pi-\theta_0}\right)} & m = 0; \ i = 0, 1, 2\cdots \\ i + \frac{\Gamma(2m+i+1)}{\Gamma(m)\Gamma(m+1)\Gamma(i+1)} \cdot \left(\frac{\pi-\theta_0}{3}\right)^{2m} & m \neq 0; \ i = 1, 2\cdots \end{cases} \tag{34}$$

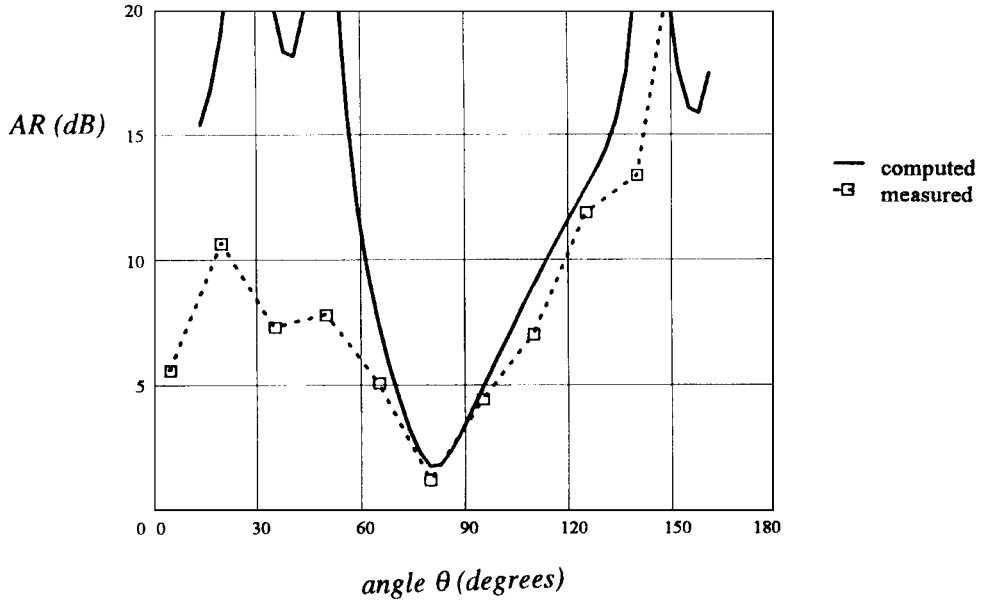

Fig. 4. The dependence of the patch axial ratio in the X–Z plane ($\phi = 0°$).

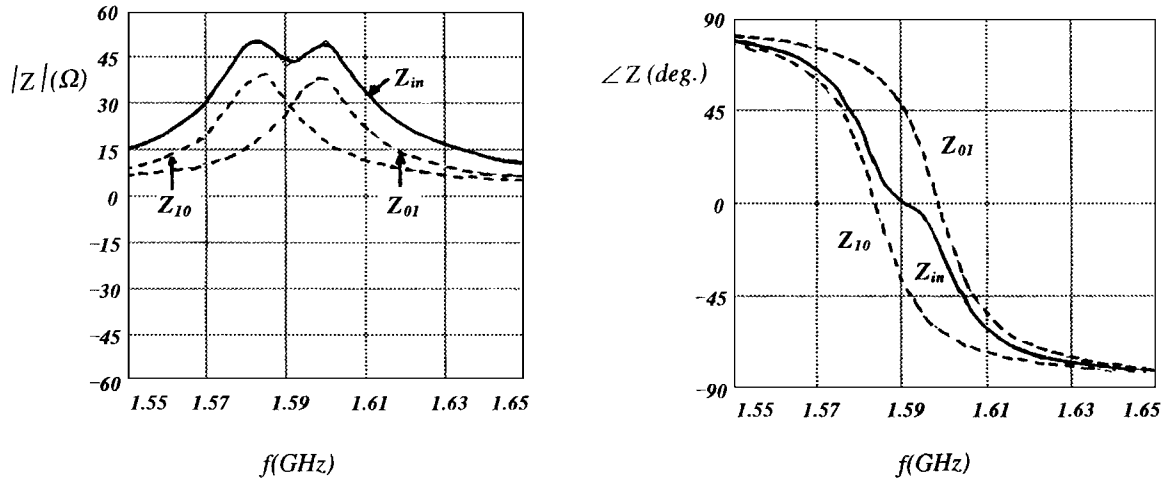

Fig. 5. Amplitude and phase of the input impedance Z_{in} and Z_{10}, Z_{01} of the dominant modes versus frequency.

to 150°. The measurement accuracy of the axial ratio depends on the absolute value of the electrical fields components; as such, for low values the accuracy deteriorates and this fact may explain the discrepancy between the measured and computed values in the range of 0° to 50°. Fig. 5 shows the amplitude and phase of the computed input impedance Z_{in} as well as the input impedances Z_{10} and Z_{01} for each of the dominant modes TE_{10}^r and TE_{01}^r excited in the cavity. One can observe that the input impedance has two peaks. This is an indicator that two modes are excited. As one can notice the resonant frequency for the TE_{10}^r mode is 1.58 GHz while that of the TE_{01}^r mode is 1.60 GHz. At the operating frequency 1.59 GHz, the phase difference between the two modes is 90° as required to generate circular polarization. Fig. 6 shows a comparison of the measured and computed data of the input impedance for feeding position $r_1 = 9.37$ cm, $\phi_1 = 6.7°$. The measured data closely follows the computed data in the vicinity of the resonance frequency. Beyond this close range, one can observe a discrepancy due to the approximations made in the measurement prototype such as the truncation of the conical surface and the dielectric substrate on which the patch is etched. All that induce additional currents, which affect the accuracy of the input impedance value of the measured patch.

IV. Summary

This paper presents a theoretical approach for the analysis of patch antennas on conical surfaces. For the computation of the input impedance we used the cavity model. In the derivation, we made some mathematical simplifications adequate for substrate thickness much smaller than the wavelength and the radius of curvature. Owing to the simplicity of the approach the input impedance was obtained with relative ease. The circular polarization was obtained by exciting in the antenna two orthogonal modes with 90° phase difference. The radiation pattern was simulated by the radiation from four magnetic

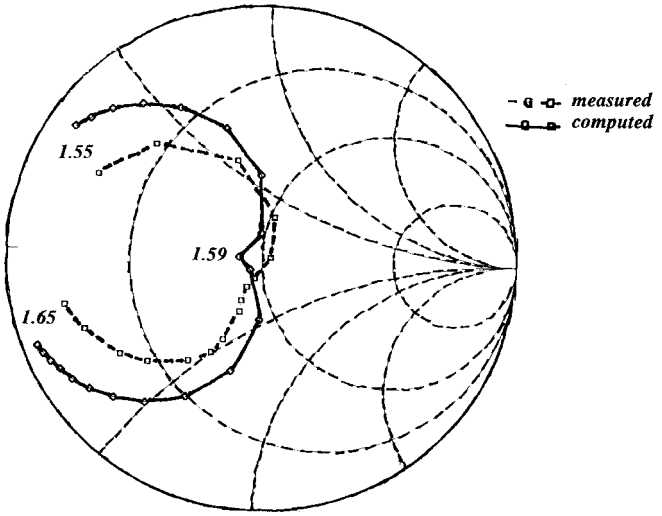

Fig. 6. Comparison between computed and measured data of the patch input impedance ($r_a = 7.68$ cm, $r_b = 10.49$ cm, $2\phi_0 = 68°$, $r_1 = 9.37$ cm, $\phi_1 = 6.7°$, $h = 0.075''$, $\varepsilon_r = 10.2$).

currents at the edges of the patch. The radiation from each magnetic current was computed using Lorentz reciprocity theorem and expansion of the field in terms of spherical modes. Some experimental data was presented to validate the theory and good agreement was shown.

ACKNOWLEDGMENT

The author would like to thank A. Lynn, Reshef Technologies, Tel-Aviv, Israel, for performing the measurements during the course of this work.

REFERENCES

[1] Y. T. Lo, D. Solomon, and W. F. Richards, "Theory and experiment on microstrip antennas," *IEEE Trans. Antennas Propagat.*, vol. AP-27, pp. 137–145, Feb. 1979.

[2] A. G. Derneryd, "Extended analysis of rectangular disk antenna element," *IEEE Trans. Antennas Propagat.*, vol. AP-27, pp. 846–849, Aug. 1979.

[3] K. M. Luk, K. F. Lee, and J. S. Dahele, "Analysis of the cylindrical-rectangular patch antenna," *IEEE Trans. Antennas Propagat.*, vol. 37, pp. 143–147, Feb. 1989.

[4] J. Ashkenazy, S. Shtrikman, and D. Treves, "Electric surface current model for the analysis of microstrip antennas on cylindrical bodies," *IEEE Trans. Antennas Propagat.*, vol. AP-33, pp. 295–300, Feb. 1985.

[5] P. Newham and G. Morris, *Handbook of Microstrip Antennas*, J. R. James and P. S. Hall, Eds. London, U.K.: Peter Peregrinus, 1989, pp. 1153–1191.

[6] J. R. Descardeci and A. J. Giarola, "Microstrip antenna on a conical surface," *IEEE Trans. Antennas Propagat.*, vol. 40, pp. 460–463, Apr. 1992.

[7] L. L. Bailin and S. Silver, "Exterior electromagnetic boundary value problems for spheres and cones," *IRE Trans. Antennas Propagat.*, vol. AP-4, no. 1, pp. 5–16, Jan. 1956.

[8] M. Kirschning, R. Jansen, and N. Koster, "Accurate model for open end effect of microstrip lines," *Electron. Lett.*, vol. 17, pp. 123–125, 1981.

[9] R. F. Harrington, *Time-Harmonic Electromagnetic Fields*. New York: McGraw-Hill, 1961, pp. 264–269.

[10] C. A. Balanis, *Antenna Theory Analysis and Design*. New York: Harper & Row, 1982, pp. 48–51.

[11] I. S. Gradshteyn and I. M. Ryzhik, *Table of Integrals, Series, and Products*. New York: Academic, 1980.

[12] M. Abramowitz and I. A. Stegun, *Handbook of Mathematical Functions*. New York: Dover, 1972.

Reuven Shavit (M'82–SM'90) was born in Romania on November 14, 1949. He received the B.S. and M.S. degrees in electrical engineering from the Technion, Haifa, Israel, in 1971 and 1977, respectively, and the Ph.D. degree in electrical engineering from the University of California, Los Angeles, in 1982.

From 1971 to 1993, he worked as a Staff Engineer and Antenna Group Leader in the Electronic Research Laboratories of the Israeli Ministry of Defense, Tel Aviv, where he was involved in the design of reflector, microstrip, and slot-antenna arrays. He was also a part-time Lecturer at Tel Aviv University, teaching various antenna and electromagnetic courses. From 1988 to 1990 he was associated with ESSCO, Concord, MA, as a Principal Engineer involved in scattering analysis and tuning techniques of high-performance ground-based radomes. Currently, he is a Lecturer at Ben-Gurion University of the Negev, Beer Sheva, Israel, doing research in microwave components and antennas. His current research interest is in the areas of tuning techniques for radomes and numerical methods for design microstrip, slot, and reflector antennas.